Mobile WiMAX handset front-end : design aspects and challenges.

Vaclav Valenta, Geneviève Baudoin, Antoine Diet, Roman Marsalek, Fabien Robert, Martha Suarez, Martine Villegas

Chapter Number

Mobile WiMAX Handset Front-end: Design Aspects and Challenges

Václav Valenta[1, 2], Geneviève Baudoin[2], Antoine Diet[3], Roman Maršálek[1], Fabien Robert[2], Martha Suarez[2], Martine Villegas[2]

[1]*Brno University of Technology, Department of Radioelectronics*
[2]*Université Paris-Est, ESIEE Paris*
[3]*Université Paris-Sud 11, UMR 8506*
[1]*Czech Republic,* [2,3]*France*

1 From the standard and regulations to front-end specifications

1.1 Regulations characteristics

The WiMAX standard includes two sub-standards. The first standard is the 802.16a or Fixed WiMAX and the second standard is the 802.16e or Mobile WiMAX. We focus here only on the Mobile WiMAX. The basic radio channel features are summarized in the Table 1.

Frequency Range (GHz)	Channel Frequency Step (kHz)	Channel Bandwidth (MHz)	FFT Size	Duplexing Mode
2.3-2.4	250	5	512	TDD
		10	1024	
		8.75	1024	
2.305-2.320 2.345-2.360	250	3.5	512	TDD
		5	512	
		10	1024	
2.496-2.69	250 (200)	5	512	TDD
		10	1024	
3.3-3.4 3.4-3.8 3.4-3.6 3.6-3.8	250	5	512	TDD
		7	1024	
		10	1024	

Table 1. Mobile WiMAX channel profiles defined by the WiMAX Forum.

The characteristics of the access modes, Wireless MAN Single-Carrier (WMAN-SCa) and Wireless MAN Orthogonal Frequency Division Multiple Access (WMAN-OFDMA) are:

- WMAN-SCa: Time Division Multiple Acces (TDMA) using following modulation techniques: BPSK, QPSK, 16 QAM, 64 QAM, 256 QAM.
- WMAN-OFDM: OFDM from 128 to 2048 carriers - modulation BPSK, QPSK, 16 QAM, 64 QAM.

For licensed frequency bands, duplex modes are both Time Division Duplex (TDD) and Frequency Division Duplex (FDD). The bandwidth is variable and it can take different values between 1 MHz and 20 MHz.

Flow rates depend on the modulation, access mode and channel bandwidths. For example, it is possible to achieve in WMAN-OFDM and OFDMA, a theoretical throughput of 73.19 Mbit/s for a band of 20 MHz, 256 carriers, using a modulation type by 64 QAM carrier .

Minimum power is: – 50 dBm for WMAN-SCa and -45 dBm for WMAN-OFDM and OFDMA. Maximum power at emission must comply with the classification:

- Class 1 : $17 \leq P(dBm) \leq 20$
- Class 2 : $20 \leq P(dBm) \leq 23$
- Class 3 : $23 \leq P(dBm) \leq 30$
- Class 4 : $30 \leq P(dBm)$

The signal integrity can be characterized by the Error Vector Magnitude (EVM). For example, WiMAX OFDMA requires a EVM less than 3.16% (for 64 QAM(3/4)) (IEEE, 2005).

2. Front-end architecture challenges

2.1 Architectures for WiMAX

Wireless communications require highly efficient and compact transceivers, whatever the signal characteristics are. In this section we focus only on the transmitter where design challenges are more critical in terms of power, size and consumption. A WiMAX transmitter architecture must meet design constraints of: providing high efficiency and linearity for a wideband OFDM (the bandwidth can be up to 100 MHz) and high Peak to Average Power Ratio (PAPR) signal (or high dynamic range) in the typical range of 20 dB (29 dB theoretical maximum). The linearization of the transmitter is mandatory because power amplification of the WiMAX signal introduces Non-Linearities (NLs) in amplitude and phase, as illustrated in Fig. 1.
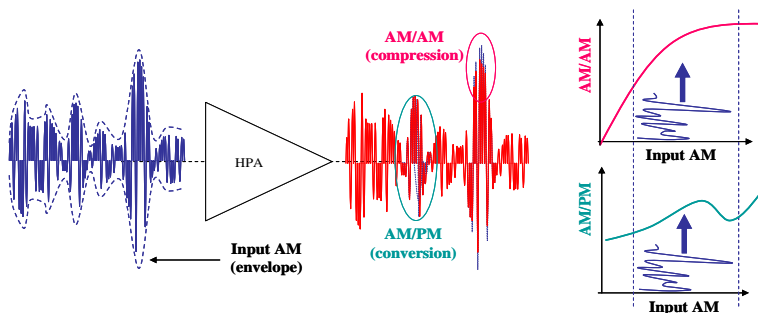

Fig. 1. Non Linearity effects of compression and conversion in high power amplification

Identifying a type of architecture for WiMAX requires a careful study of linearization techniques and their performance with wideband and high dynamic range signals. There

are several linearization techniques depending on the PAPR of the signal, the added complexity and the increase in size and consumption of the system that can be accepted by the designers (Villegas et al., 2007). Many criteria characterize the linearization techniques such as static/dynamic processing, adaptability, frequency (digital, baseband, IF or RF), memory effect correction, complexity, stability, resulting efficiency, size increase etc. Herein, for WiMAX application, we basically classify these techniques in three groups: (i) correction techniques, (ii) anticipation of NL and (iii) those based on a decomposition and recombination of the signal, often dedicated to wideband signals.

Examples of correction techniques are feed-back (*A*), feed-forward (*B*) and the anticipation technique principle of pre-distortion (*C*) (see Fig. 2). Their common point is to add a modification/correction to the modulated signal (before or after) at the Power Amplifier (PA) stage. The architecture considerations here do not include the modulator nor the baseband signal processing. This needs a carefully derived model of the PA non-linear effects (Volterra series, Wiener or Saleh model etc.). Adaptability to the signal amplitude can be introduced in order to compensate for the lack of accuracy in the NL effects model and memory effects of the PA (also temperature drift compensation can be considered) (Baudoin et al., 2007).
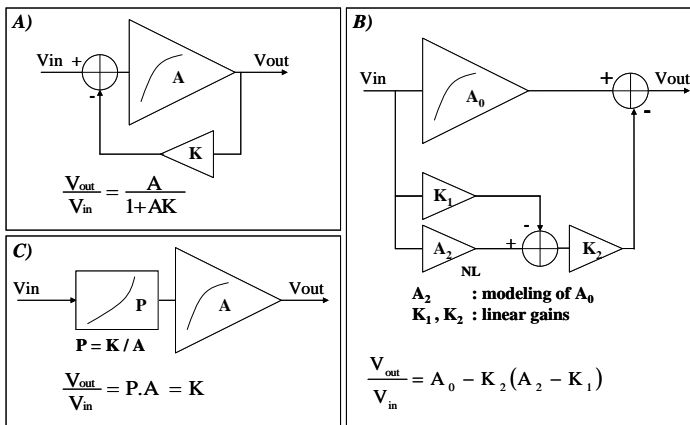

Fig. 2. Principles of feed-back (*A*), feed-forward (*B*) and pre-distortion (*C*).

Each structure contains a major defect. Feed-back (*A*) reduces the gain of the amplification and introduces a bandwidth limitation due to the transfer function of the loop (stability and dynamic response). The feed-back can be realised on the amplitude (Polar feed-back) or on I and Q quadrature components of the signal (Cartesian feed-back) and both are dedicated to narrowband signal linearization. Feed-forward (*B*) requires a significant increase in signal processing and RF blocks in the transmitter, with the hypothesis of a precise matching between NLs and reconstructed transfer functions. The improvement in linearity will be expensively paid for in terms of consumption and size (integration). Advantages are the stability and possibility to process wideband signals. The most interesting is pre-distortion (*C*) because of its flexibility: the anticipation can be done in the digital part and so provide adaptability of the technique, but this needs a feed-back loop. The digital pre-distortion represents a non-negligible additional consumption of a Digital Signal Processor (DSP) and

often requires a look up table. The signal is widened in frequency because of the expensive non-linear law of the pre-distorter (as for IPx theory on a modulated signal spectrum), requiring baseband and RF parts to be wideband designed. Interesting improvements of pre-distortion have been made with OFDM signals in (Baudoin et al., 2007).

Others techniques presented are based on a vectorial decomposition of the signal in order to drive high efficiency switched mode RF PAs with constant envelope (constant power) signals, avoiding AM/AM and AM/PM (Raab et al., 2003); (Diet et al., 2003-2004). These techniques are dedicated to correcting strong NL effects. We consider the problem of linearization in the communication chain from the digital part to the emission. This drives for a complete modification of the architecture and its elements' specifications in baseband, RF and power RF. After amplification of constant envelope parts of the signals, the difficulty is to reintroduce the variable envelope information with lower NL than in a direct amplification case, while maintaining the efficiency of the architecture. Basic examples of these techniques are the LInearization with Non Linear Components (LINC) and the Envelope Elimination and Restoration (EER) methods (and theirs recent evolutions) (Cox, 1974); (Kahn, 1952); (Diet et al., 2004).

The LINC principle relies on a decomposition of the modulated signal into two constant envelope signals as is shown in Fig. 3. The decomposition can be computed by a DSP or by combining two Voltage Controlled Oscillators (VCOs) in quadrature locked-loop configuration (CALLUM). CALLUM is an interesting architecture but presents a possibility of instability and additional costs of realisation. The amplification of the two constant envelope signals drives for the design of two identical High Power Amplifiers (HPAs) at the RF frequency, and often causes signal distortion due to imbalance mismatch. Also the HPA has to be wideband because the signal decomposition is a non-linear process, and the phase modulation ratio is increased.

$$I + j.Q = R(t).e^{j\Phi(t)}$$
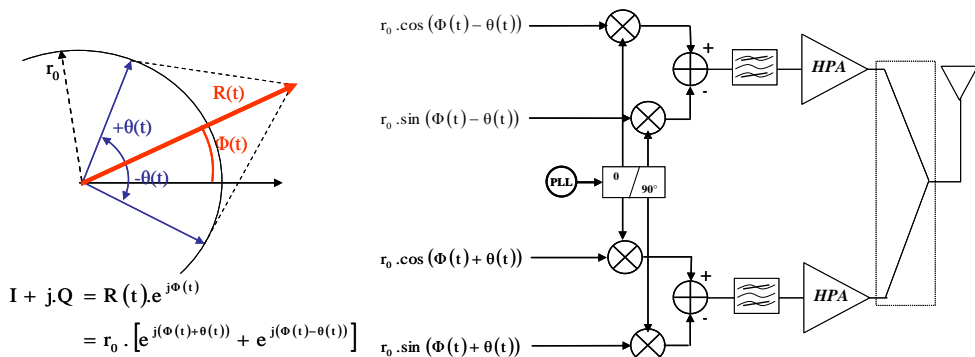$$= r_0 . \left[e^{j(\Phi(t)+\theta(t))} + e^{j(\Phi(t)-\theta(t))} \right]$$

Fig. 3. LINC decomposition and recombination at RF power amplification.

Whatever the decomposition technique is (LINC/CALLUM), the default is that efficiency is directly determined by the recombination sum operation. It is very difficult to avoid losses at high frequency while designing a RF power combiner.
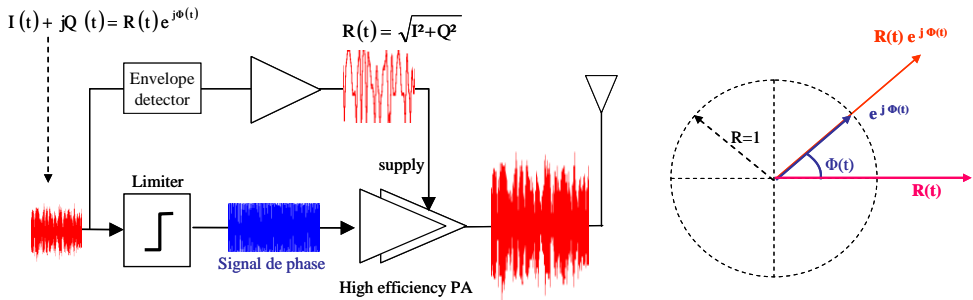
Fig. 4. Principle of the EER technique (Kahn, 1952).

Another decomposition technique was proposed by Kahn in 1952 and is basically an amplitude and phase separation: EER. This method was first proposed for AM signals as represented in Fig.4. The advantage of EER is to drive the RF PA with a constant envelope modulated signal (carrying the phase information), enabling the use of a switched and high efficiency amplifier (Raab et al., 2003); (Sokal & Sokal, 1975); (Diet et al., 2005-2008). The difficulty is to reintroduce the amplitude information using the variation of the PA supply voltage. This implies a power amplification of the envelope signal, at the symbol rate frequency. The recombination can be done with high efficiency switched (saturated) class PA because their output voltage is linearly dependant on the voltage supply. Synchronisation between the phase and the amplitude information and linear amplification of the amplitude before the recombination are the two difficulties of such a linearization technique as reported in (Diet, 2003-2004) where a maximum delay of 3 nanoseconds during the recombination of an 20 MHz OFDM 802.11a signal causes spectral re-growth of more than 40 dBc (standard limit) at 30 MHz from the carrier frequency (5 GHz). Recently, a lot of work has been done on the EER based architectures, often classified as polar architectures (Nielsen & Larsen, 2007); (Choi et al., 2007); (Suarez et al., 2008); (Diet et al., 2008-2009). The generation of the amplitude and phase components can be expected to be done numerically thanks to the power of DSPs as is shown in Fig. 5. As was previously discussed in (Diet et al., 2003), the bandwidths of the envelope and phase signals are widened and make it necessary to design the circuit for three to four times the symbol rate.

101010   CNA

$R(t) = \sqrt{I^2 + Q^2}$

PWM or
ΣΔ coding

D
E
C
O
M
P
O
S
I
T
I
O
N

001101   CNA

$\cos(\Phi) = \dfrac{I}{\sqrt{I^2 + Q^2}}$

011001   CNA

$\sin(\Phi) = \dfrac{Q}{\sqrt{I^2 + Q^2}}$
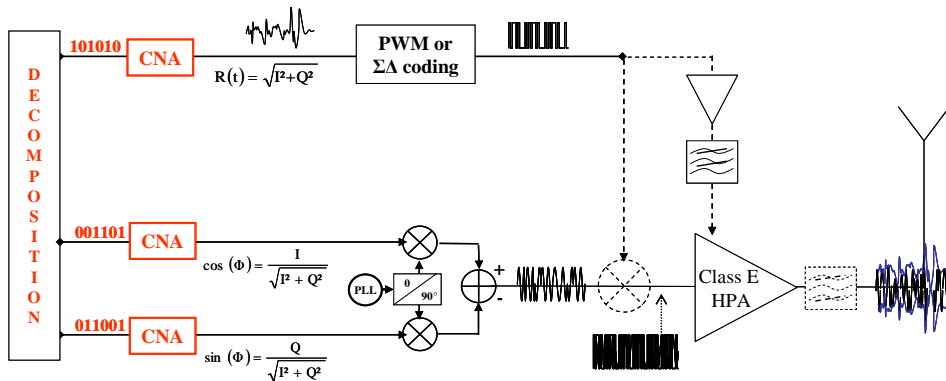
PLL   0   90°

+
-

Class E
HPA

Fig. 5. Recent improvements of EER/polar architectures for wideband OFDM signals.

For a WiMAX signal, such a technique requires in the range of a hundred MHz bandwidth on the phase and amplitude baseband paths (as for LINC technique and any other non-linear decomposition method). Since a clipping in frequency and on the envelope is possible, they are suited for new high data rate standards such as WiMAX, where efficiency of the emitter and linearization are mandatory. Also, the multi-standards and multi-radio concepts evolved the polar architectures in multiple ways (Diet et al., 2008). For example, the recombination on the drive signal of the PA is possible because the amplitude information modulates the phase RF signal and is restored by the band-pass shape function of the following blocks: PA + emission filter + antenna. The emitted spectrum is the criterion of quality to be considered carefully, because the Pulse-Width Modulation (PWM) or ΣΔ envelope coding are the source of useless and crippling spectral re-growth. The efficiency is also penalized by the power amplification of such useless components but this is balanced by the advantage of high flexibility of this architecture (Robert et al., 2009). Actual work is focused on the front end design to provide the highest efficiency possible with the PA driven signal composed by the phase and amplitude coded information. The digitally controlled PA and the mixed-mode digital to RF converter performance are key parameters in the evolution of polar architectures (Suarez et al., 2008); (Robert et al., 2009); (Diet et al., 2008).

To summarize, WiMAX architecture is expected to be wideband and high efficiency due to the signal characteristics. Polar based architectures seem to be the best candidate at the moment and corresponds to the actual focus in radio-communication research topics. The high performance of digital adaptive pre-distortion techniques on OFDM signals should be noted. It is later of interest in a polar/pre-distorted mixed linearized technique.

2.2 PAPR and its reduction

As mentioned above, the OFDM signals suffer from the high envelope dynamics, characterized by the PAPR. The PAPR of an OFDM signal with N subcarriers sampled at the symbol rate is upper-bounded by the value N (about 24 dB for a mode with 256 subcarriers). Most of the time, the instantaneous value of the PAPR is much lower. Statistically it is possible to characterize the PAPR distribution (probability that the PAPR exceeds a given

threshold γ) using the Complementary Cumulative Distribution Function (CCDF). For the case of OFDM, the following expression for the PAPR CCDF holds (Nee & Prasad, 2000):

$$\Pr(\text{PAPR} > \gamma) = 1 - (1 - \exp(-\gamma))^N \tag{1}$$

The PAPR reduction methods can be categorized into two general groups - the methods introducing signal distortion and the distortionless methods. The simplest method from the former group is the clipping. In its basic form, this method simply clips the signal magnitude to the desired maximal level. In this case the PAPR is reduced at the expense of signal distortions resulting in out of band emissions and BER increase. In order to suppress these effects, the research was directed towards more advanced methods like repeated clipping and filtering etc.

Many techniques that do not introduce the distortions have been proposed in the past. The Selective Mapping (SLM) is based on the creation of several alternative signal representations of the original input data, bearing the same information (LIM et al., 2005). The one with the lowest PAPR is selected for transmission. In the Partial Transmit Sequences (PTS) (Mäuller & Huber, 1997) method, the IFFT input symbols are divided into several frequency disjoint sub-blocks. The output of each sub-block is multiplied by the complex rotation factor. These factors are optimized in order to find the variant with the lowest PAPR.

Moreover, methods like the tone reservation or tone injection, belonging to the group of so-called additive methods (Tellado, 2000), can be used.

The PAPR CCDF's of OFDM system corresponding to WiMAX modes with the FFT size of 128, 256, 512, 1024 and 2048 are shown in Fig. 6. The PAPR improvement resulting from the use of PTS (4 sub-blocks, rotation factors being either 1 or -1) and SLM (6 alternatives) methods is shown for the illustration in the same figure for the case of FFT size equal to 256.

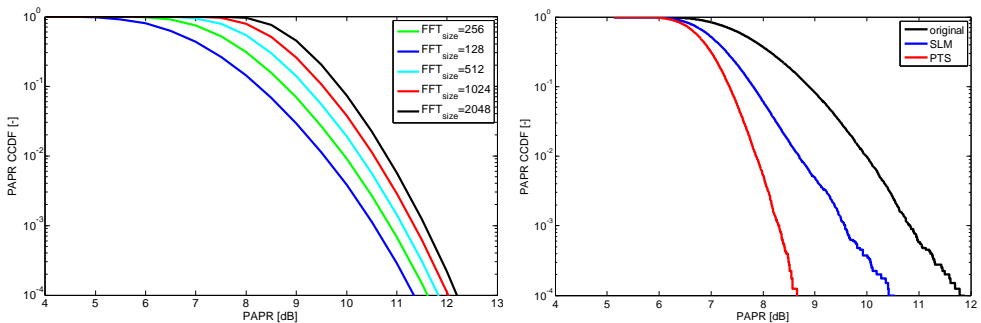Fig. 6. Theoretical PAPR CCDF for WiMAX modes with FFT size from 128 to 2048 (left) and the PAPR improvement due to use of PAPR reduction for FFT size equal to 256 (right)

2.3 Integration technologies: System-in-Package (SiP) or System-on-Chip (SoC)
Due to the increasing complexity of integrated circuits and systems, new packaging technologies are developed. Their choices shape the design of elementary circuits.

Three constraints are essential to take into account in the design and integration of architecture transceiver:

- Improving performances
- Circuit size
- Energy consumption

while controlling costs.

To tackle these challenges, the silicon integration and the packaging must be taken into account when designing systems.

SoC have different digital and analog functions live on the same chip. It is a full integration on silicon. SoC technology combines collectively processed components on the same chip, and using compatible processes. It is more complex to design but can achieve more competitive prices for major production.

The overall reliability is also improved. But today, some functions such as filtering and power amplification can not be used SoC technology, particularly for WiMAX systems.

The system must be divided into functions. This technique requires co-design. The chips are then assembled using a specific connection technology. The design constraints are released but the unit cost is higher. The reliability is lower and the operating speed of circuits may decrease depending on the chosen connection technology.

3. Frequency Synthesis for Mobile WiMAX Radios

Unlike 2G and 3G wireless communication systems with a fixed channel bandwidth, the Mobile WiMAX standard enables a variable channel size and multiple frequency allocation, and thereby offers very flexible deployment. As a result of multi-wideband operation, a high performance RF front-end has to be employed. One of the most challenging RF blocks to design in a radio front-end is undoubtedly the frequency synthesizer. The frequency synthesizer acts as a Local Oscillator (LO) generation unit that is used to translate baseband and RF signals by means of mixing and it frequently determines the overall performance of a radio communication system. Evaluation of the frequency synthesizer's complexity and requirements relates to the WiMAX RF architecture. WiMAX considers three RF architectures, TDD, FDD and Half FDD (HFDD). Since the TDD mode utilizes a single frequency band for the uplink and downlink direction, only one local oscillator is required. Contrary to the TDD, the FDD mode requires two separate synthesizers for RX and TX due to the full duplex nature of the architecture and hence, switching requirements can be relaxed. However, the overall complexity of the FDD front-end leads to larger RFIC due to additional circuitry, higher power consumption and most importantly, to higher costs of implementation. Therefore, the TDD architecture is more suitable for the mobile version of the WiMAX standard.

Multi-carrier OFDM scheme, which is employed in WiMAX, has become very popular in wideband communication systems as it offers very high spectral efficiency and can efficiently combat selective fading resulting from multipath propagation (Cimini, 1985). High spectral efficiency is achieved by parallel low-rate narrowband modulation of orthogonal sub-carriers equally spaced by $\Delta f = 1/T_u$, where T_u is the useful symbol length

(length of the FT interval). In the ideal case, all sub-carriers are orthogonal, in other words, they don't interfere with each other. Therefore, an inter-carrier guard interval commonly used in frequency-division multiplexing is not required. However, as the sub-carriers are very close together, the OFDM signal becomes less resilient to frequency errors, namely to inaccuracies such as Doppler shift and LO phase noise (Muschallik, 1995); (Zou et al., 2007). The phase noise introduced by the frequency synthesizer can be interpreted as a parasitic phase modulation of the LO carrier that is subsequently superimposed on individual OFDM sub-carriers as a result of the frequency translation (up and down conversions). This parasitic phase modulation causes significant degradation of the OFDM signal and may lead to the loss of orthogonality as a result of Inter-Carrier Interference (ICI). The effect becomes even more harmful as the number of sub-carriers increases in a given bandwidth, because the length of the OFDM symbol T_u gets longer, making the system more sensitive to the LO phase noise. However, longer symbols increase spectral efficiency of an OFDM system, and therefore, these parameters have to be compromised.

There exist two different effects of the LO phase noise on the OFDM signal: Common Phase Error (CPE) resulting from the LO noise contribution present within the sub-channel. CPE affects all sub-carriers in the same manner and can be observed as a common rotation of all constellation points in the I/Q plane (Muschallik, 1995). Other phenomenon is ICI, which results from the adjacent LO noise contribution.

Correlation between the integrated phase noise (phase jitter) and the bit error ratio (BER) degradation has been reported in (Muschallik, 1995); (Herzel et al., 2005); (Armada, 2001). In order to eliminate this impact, phase noise of the OFDM synthesizer has to be optimized according to the maximum allowed phase noise or phase jitter (for a given BER).

3.1 Frequency synthesizer requirements

The frequency synthesizer has to provide the range of all necessary frequencies with proper channel spacing that corresponds to the channel raster. WiMAX channel profiles are summarized in Table 1 (WiMAX Forum, 2008). The channel frequency step given by the WiMAX standard is 250 kHz, however, the LO has to deliver the required frequency with a resolution of 125 kHz as a result of raster overlapping for different channel bandwidths (WiMAX Forum, 2008). Another directive parameter for design is the tuning range and the frequency settling time. Frequency switching time between RX and TX in the HFDD mode has to be performed agilely, with respect to settling time requirements of the standard, which is to be less than 50 µs. Moreover, the local frequency synthesizer has to fulfil the tightest signal purity requirements that can be expressed in terms of the integrated phase noise and the spurious output. The integrated phase noise is to be less than 1 deg rms within an integration frequency of 1/20 of the tone spacing (modulated carrier spacing) to ½ the channel bandwidth (Eline et al., 2004). Thus for smaller channel bandwidths the integration of the phase noise can start from as low as a few hundred Hertz.

To satisfy very high requirements imposed by the WiMAX whilst at the same time benefiting from the ease of integration and flexibility, fractional-N Phase Locked Loop (PLL) based architecture becomes the appropriate design option. Fractional-N PLL can achieve very small frequency resolution equal to the fractional portion of the reference frequency and hence improve the phase noise performance by a factor of 20log (N) compared to the conventional integer-N PLL (Keliu & Sanchez-Sinencio, 2005).

3.2 High-speed frequency synthesizer design example

Fractional-*N* synthesizers have become very popular and widely used in a range of RF applications because they allow the comparison Phase Frequency Detector (PFD) frequency f_{PFD} to be significantly higher than the required frequency resolution (Keliu & Sanchez-Sinencio, 2005). Higher PFD frequency automatically leads to wider loop bandwidth (as the loop bandwidth is to be < $0.1f_{PFD}$) and therefore significantly improves settling time performance compared to the integer-*N* PLL. Moreover, since the Mobile WiMAX standard defines the channel raster resolution as 125 kHz, the PFD frequency of an integer-*N* synthesizer would have to be as low as 125 kHz and hence, the division factor *N* would reach up to 30,400 in order to generate the highest frequency of 3.8 GHz (Valenta et al., 2008). This would, in turn, deteriorate the in-band phase noise contribution by up to 48 dB, compared to the fractional-*N* synthesizer with a reference frequency of 32 MHz (where *N*≈119, assuming the same phase noise performance of both reference clocks).

In the next example, we consider a fractional-*N* Charge Pump (CP) frequency synthesizer as an application for the 3.4 – 3.8 GHz channel profile. A simplified model is depicted in Fig. 7. This model includes a tri-state PFD that produces output *up* and *down* signals, proportional to the phase and frequency difference between the reference and the feedback signal. PFD employs two positive edge-triggered resetable FF (flip-flop) to detect the phase and frequency difference and one AND gate to monitor the *up* and *down* signals. The upper FF is clocked by f_{ref}, the lower by f_{div}. Signals *up* and *down* are used to switch the current sources in the CP. These CP current pulses change the voltage drop on the loop impedance and tune the VCO with tuning gain of 125 MHz/V and tuning range of 3.4-3.88 GHz. The fractional division is achieved by altering the division value between two integer values *N* and *N*+1, hence the average division becomes a fraction. However, the periodic switching between two division values leads to a sawtooth phase error, which can create spurious fractional tones. This problem is solved with help of ΔΣ modulator, which randomize the switching between *N* and *N*+1, but on the other hand, it introduces quantization noise into the loop.
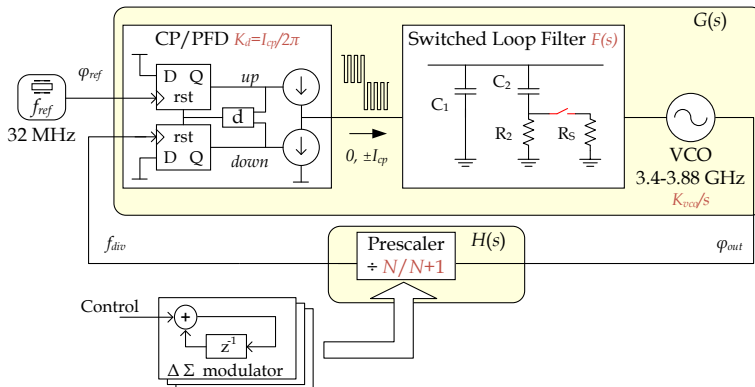

Fig. 7. General model of the fractional-*N* charge pump synthesizer.

The loop filter is the key component of the PLL and it characterizes the dynamic performance of the synthesizer. Loop filter design involves choosing the proper loop filter

topology, loop filter order, phase margin and loop bandwidth. Due to low phase noise requirements set by the Mobile WiMAX standard, a passive filter has been chosen. The trade-off between the minimum loop bandwidth and the settling time has to be taken into account for optimal loop filter design. A simplified trade-off presented by (Crawford, 1994) is $B_{PLL} = 4/t_{lock}$, where t_{lock} is the settling time. Applied to WiMAX, the PLL would call for at least 200 kHz loop bandwidth in order to settle within 20 μs. However, such a wide PLL bandwidth would result in a very high in-band phase noise integration and phase jitter deterioration.

A significant settling time improvement can be achieved by means of loop filter switching (Crowley, 1979). The loop filter is switched to the fast wideband mode during the frequency transition and then, after a certain programmable period, is shifted back to the normal narrowband value. To understand the switching principle, let us have a look at the PLL control theory and the PLL linearized model. The effect of a closed feedback loop on the input reference signal φ_{in} can be described by the closed loop transfer function $T(s)$ as:

$$T(s) \; = \; \frac{\varphi_{out}(s)}{\varphi_{in}(s)} \; = \; \frac{G(s)}{1 \; + \; G(s)H} \; = \; \frac{\dfrac{K_d K_{vco}}{s} F(s)}{1 \; + \; \dfrac{K_d K_{vco}}{s} F(s) \dfrac{1}{N}} \qquad (2)$$

where the $G(s)$ represents the open loop transfer function and H corresponds to the division factor $1/N$. K_d is the gain of the CP/PFD detector and equals to $I_{cp}/2\pi$, K_{vco} is the VCO gain in MHz/V and $F(s)$ refers to the transimpedance of the second order loop filter as depicted in Fig. 7.

$$F(s) \; = \; \frac{1 \; + \; s C_2 R_2}{s(C_1 \; + \; C_2)\left(1 \; + \; s \dfrac{C_1 C_2 R_2}{C_1 \; + \; C_2}\right)} \qquad (3)$$

The angular open loop crossover frequency ω_c and the phase margin θ_c are defined at the point where the magnitude of the loop gain reaches unity. This can be expressed as $\|G(s)H\| = 1$ (0 dB), where

$$G(s)H \; = \; \frac{K_d K_{vco} F(s)}{sN} \; = \; \frac{I_{cp} K_{vco} F(s)}{2\pi s N} \; , \qquad (4)$$

$$G(s)H\Big|_{s=j\omega_c} \; = \; -\frac{I_{cp} K_{vco}}{2\pi \omega_c^2 N} \frac{1 \; + \; j\omega_c T_2}{1 \; + \; j\omega_c T_1} \frac{1}{C_1 \; + \; C_2} \; . \qquad (5)$$

And then, the open loop phase margin θ_c at the crossover frequency ω_c reads

$$\theta_c\,[rad\,] \; = \; \pi \; + \; \arctan(\; \omega_c T_2) \; - \; \arctan(\; \omega_c T_1) \; . \qquad (6)$$

T_2 and T_1 correspond to time constants of zero and the pole in the loop filter transfer function respectively ($T_2 = C_2 R_2$, $T_1 = C_1 C_2 R_2 / (C_1 + C_2)$).

Let us consider a situation, where the crossover frequency ω_c is increased by factor a in order to increase the loop bandwidth and thereby decrease the settling time. This adjustment is applied only during the frequency transition. To ensure the loop stability at $a \cdot \omega_c$, the phase margin θ_c defined by the equation (6) has to remain constant. This can be done by means of reducing the value of T_2 and T_1 by the factor a with help of a parallel resistor $R_s = R_2 / (a-1)$. as displayed in Fig. 7. Moreover, the product of all elements in (5) has to be increased by factor of a^2 as the angular frequency ω_c in (5) is in the power of two. This can be done by means of increasing the charge pump current I_{cp} by factor a^2. In this example, we consider $a = 4$ and therefore, to activate the fast wideband mode, the CP current is increased by a

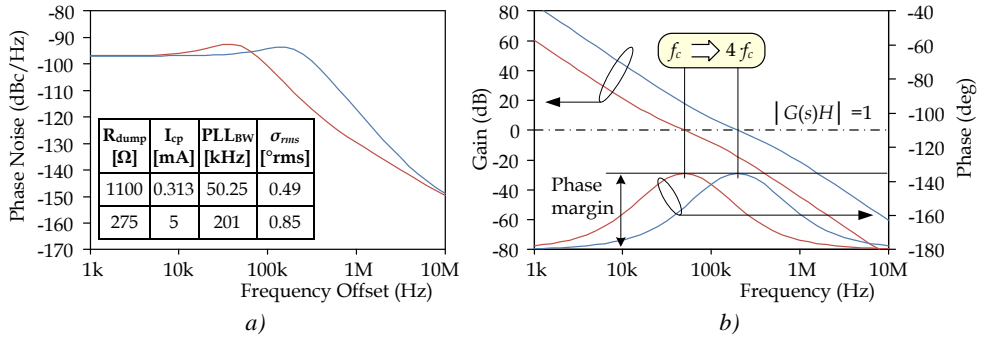| R_{dump} [Ω]	I_{cp} [mA]	PLL_{BW} [kHz]	σ_{rms} [°rms]
1100	0.313	50.25	0.49
275	5	201	0.85

a) *b)*

Fig. 8. Phase noise performance (*a*) and the open loop gain with the phase (*b*) at 3.59 GHz. The blue line corresponds to behaviour during the frequency transition (wideband mode).

factor of 16 ($I_{cp} \rightarrow 16 \cdot I_{cp}$), while reducing the dumping resistance by a factor of 4 (by using a parallel resistor R_s). The PLL open-loop crossover frequency, the zero and pole frequency ($1/R_2 C_2$ and $1/[R_2 C_1 C_2 / (C_1 + C_2)]$) are all increased by a factor of 4 while the loop stability remains unaffected (see the constant phase margin in Fig. 8 *b*). Figure 8 *a*) shows the phase noise performance and the resulting phase jitter of the dual bandwidth adjustment. Phase jitter of both loop configurations has been calculated as

$$\sigma_{rms} [°] = \frac{180}{\pi} \sqrt{2 \int_{f1}^{f2} S(f) df} \quad , \tag{7}$$

where $S(f)$ is the total phase noise at the PLL output. f_1 and f_2 correspond to the integration borderers (from 1/20 of the carrier spacing to half the bandwidth). Figure 9 presents the settling time improvement that has been achieved by means of loop filter switching. The settling time has dropped from 88 µs to 32 µs (settling time within 100 Hz).
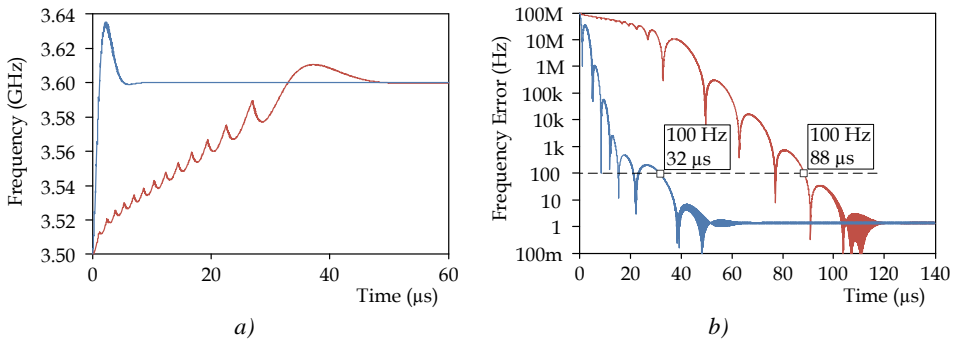
Fig. 9. Transient responses of the fast PLL for two cases: wideband mode enabled/disabled (blue/red line respectively). Plot *b)* displays the absolute frequency error in reference to the settling frequency of 3.6 GHz.

3.3 Hybrid PLL approach for frequency synthesis

The product of all elements in Equation (5) can be changed not only by increasing the I_{cp}, but also by simultaneous altering of the feedback division factor N and the I_{cp}. However, by altering the division factor in the feedback path, the output frequency will shift as well. To keep the output frequency constant either during the transition, or once in the stable mode, the hybrid fractional/integer PLL approach has to be considered (Memmler et al., 2000); (Kyoungho et al., 2008). The fractional-*N* wideband mode is enabled along with the loop switching during the frequency transition and then, after settling, the integer-*N* narrowband mode is turned on. This approach brings a new degree of flexibility and alleviates CP requirements in terms of the I_{cp} current range by reducing the division ratio N. In a very particular situation, the bandwidth can be switched only by altering the feedback division factor and the dumping resistance while keeping the I_{cp} constant. In the fast wideband fractional-*N* mode, the additional dividers (*x*–labelled blocks in Fig. 10) are not employed and the reference frequency as well as the feedback signal is applied directly to the PFD. After settling, the integer-*N* mode is enabled by switching the loop bandwidth to the normal narrowband value and by activating two additional dividers. The additional division ratio x is chosen such that the PFD frequency corresponds to the required frequency resolution. Applied to the previous example where a 32 MHz reference is used, the division x has to be 256, in order to achieve 125 kHz resolution. The wideband fractional mode is then enabled by switching the resistance R_s and by disabling both dividers. This adjustment results in boosting the loop bandwidth by factor 16 while keeping the I_{cp} constant. The stability is not affected since $R_s = R_2/(a-1)$, where $a = \sqrt{256}$ and at the same time the ratio I_{cp}/N is increased by factor a^2; $\{I_{cp}/(N/a^2)\}$.

The hybrid approach inherits the speed performance from the fractional-*N* PLL and at the same time the design simplicity of the integer-*N* PLL (the $\Delta\Sigma$ modulator can be replaced by an accumulator because the fractional spur reduction is not needed during the transient period). Moreover, a higher loop bandwidth enlargement is possible compared to the conventional bandwidth switching (where only I_{cp} and R are altered). On the other hand, the main drawback of the hybrid architecture is evident: the phase noise performance of such a synthesizer corresponds to the performance of an integer-*N* synthesizer, which has inherently worse phase noise performance compared to the fractional-*N* architecture.

Due to the high degree of flexibility and integrability, the hybrid PLL approach is a very promising choice for multi-standard and multi-band transceivers, where different standards impose different requirements in terms of phase noise, settling time or channel raster.
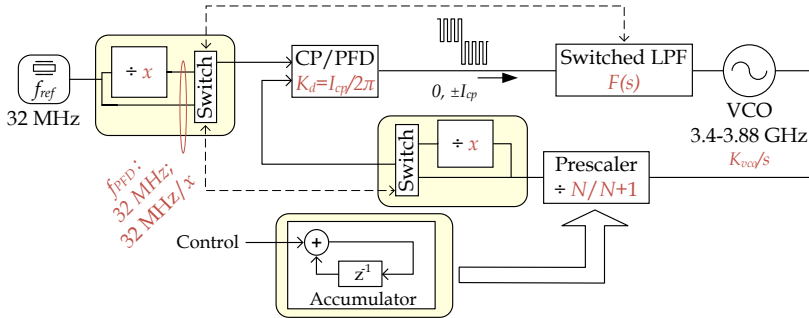

Fig. 10. Functional scheme of the hybrid PLL synthesizer.

4. High Performance Power Amplifier Design for Mobile WiMAX Radios

4.1 Transistor technology
The technologies available to realize integrated circuits in the WiMAX bands are as follows. Gallium Arsenide (GaAs), which allows high operating frequencies and high output power to be achieved. This technology is generally used for power amplifiers and switches. The manufacturing cost is higher compared to silicon. Using this technology requires a SiP packaging.

Silicon technologies are numerous: silicon bipolar transistor, CMOS, BiCMOS etc. Under certain conditions, they can achieve good performances, up to tens of GHz. A final interesting technology is the SiGe that may eventually replace the GaAs for some functions.

Figures of merit are classically used to describe RF and microwave transistors characteristics. They are used by a designer to compare technologies performances. Two frequency characteristics are used: the cutoff frequency f_t, and the maximum oscillation frequency f_{max}. These frequencies define the upper limits of component operation. They are particularly important for low noise or power devices.

The cut-off frequency f_t is defined when the amplitude of the current gain (H_{21}) is equal to 1 (0 dB) if the output presents short circuit. The maximum oscillation frequency f_{max} is defined when the unilateral power gain is equal to 1 (0 dB).

For RF or microwave integrated circuit design, f_t and f_{max} must be as high as possible. A rule is to give an operating frequency equal to the maximum f_t divided by ten.

There are other electrical characteristics used depending on the application. The minimum noise factor, N_{fmin}, given in dB at the working frequency, it is important for all low-noise components. The output power P_{out}, given in dBm or W, is important for power components. For such power applications, it is also important to define the output power density, expressed in watts per millimetre gate development in the case of field-effect transistors, and emitter surface in the case of bipolar transistors.

4.2 Continuous Wave (CW) Classes

Power Amplifiers in RF applications such as WiMAX are designed to linearly amplify high dynamic signals with high efficiency, due to the consideration of the battery lifetime. They are loaded by the emission filter and/or the antenna and deliver a RF power that can reach 27 to 30 dBm. In that context, the performance evaluation criteria are the spectral re-growths as a form of measure of the linearity (linked to the Adjacent Channel Power Ratio (ACPR) and to the Adjacent Channel Leakage Ratio (ACLR), the factor of use *Fu* as a technological aspect for the design, see (8), and the efficiency of operation; see (9) for drain/collector η and (10) for added efficiency η_{AE}. Topologies of PAs are presented here in the case of common emitter with RF MESFET design for simplicity and can be easily adapted to BJT, HBT, (LD)MOS or x-HEMT transistors.

$$Fu = \frac{V_{max} \times I_{max}}{P_{RF\_out}} \qquad (8)$$

$$\eta = \frac{P_{RF\_out}}{P_{DC}} \qquad (9)$$

$$\eta_{AE} = \frac{P_{RF\_out} - P_{RF\_in}}{P_{DC}} \qquad (10)$$

PAs are grouped in several classes of operation. A class is determined by (i) the polarisation of the transistor, (ii) the wanted shape of the output signal (voltage and current) and (iii) the hypothesis on transistor saturation (current source or switch behaviour). There are two families of PA classes: the switched class (SW), discussed in the following section, and the CW or biased class. A CW class is characterised by the polarisation point of the transistor, implying the conduction angle (θ) of the PA, as illustrated in Fig. 11.
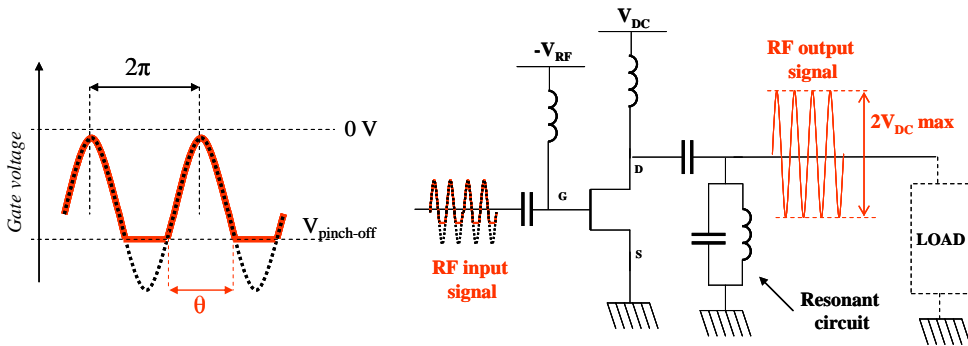
Fig. 11. Angle of conduction and polarization of a CW MESFET PA.

The PA classes with $\theta \geq \pi$, are class A (2 π), AB (2π > θ > π,) and B (π). Their main characteristics are that the PA dissipates power whatever the amplitude of the signal, and therefore the maximum efficiency is obtained at maximum linear amplitude of the output voltage. For class C (< π) the dissipated power is non-linearly proportional to the input

signal amplitude and increases with the reduction of θ. Equations of the maximum efficiency as a function of the conduction angle $\theta = \theta_c$ are based on the analysis of (Krauss et al., 1980) and are summarised by (11), (12) and (13) and in Fig. 11.

$$V_{RF} \;=\; \frac{V_p}{\cos\left(\dfrac{\theta_c}{2}\right) \;-\; 1} \tag{11}$$

$$\eta \;=\; \frac{P_{RF}}{P_{DC}} \;=\; \frac{\theta_c \;-\; \sin(\theta_c)}{4.\left(\sin\left(\dfrac{\theta_c}{2}\right) \;-\; \dfrac{\theta_c}{2}.\cos\left(\dfrac{\theta_c}{2}\right)\right)} \tag{12}$$

$$Fu \;=\; \frac{V_{max}.i_{RF}\left(1-\cos\left(\dfrac{\theta_c}{2}\right)\right)}{P_{RF}} \;=\; \frac{8\pi\left(1 \;-\; \cos\left(\dfrac{\theta_c}{2}\right)\right)}{\theta_c \;-\; \sin(\theta_c)} \tag{13}$$
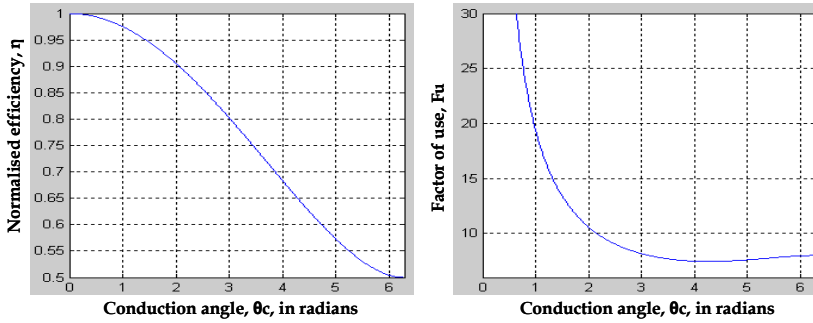

Fig. 12. Efficiency and Factor of use of CW classes.

It is important to consider that the efficiency is given as a peak value for CW classes. For an AM signal the average efficiency will rely on the amplitude information statistic, if there is no saturation. An improvement in efficiency is gained if saturation/clipping on the peak values is introduced in order to increase the average power of the output signal for the same power dissipated by the amplifier. The amplifier gain is dependant on the load line and so also on θ. Gain and linearity reduce while the efficiency increases. The WiMAX signal presents such a high PAPR that the amplification by a CW class PA requires a low efficiency back off or a linearization technique to reduce the non-linear effects of compression and conversion introduced by the saturation. Techniques interesting for wideband and high PAPR signal are those using the highest efficiency PAs. A way to improve CW efficiency is to saturate class B or class C PAs as described in (Krauss et al., 1980) as the mixed mode class C/C*. In fact, the saturation of the PA corresponds to the use of the transistor as a switch and not as a classical current source. The amplification of amplitude information by

the driving input signal becomes impossible in this mode. SW class PAs are based on this principle.

4.3 SW Classes

SW classes are based on the hypothesis that the transistor switches perfectly. This latter is supposed to act as a current source and as a voltage source alternately with non-overlapping, which would result in dissipated power (Krauss et al., 1980); (Raab et al., 2003), see Fig. 13. The filtering is mandatory in RF applications, except if the SW PA is dedicated to the amplification of a square signal, which is class D. When the square signal is low-pass filtered in order to recover a PWM or other pulse-coded information (ΣΔ), the amplifier is often named a class S amplifier. The load line of every SW PA class tends to be that of an ideal switch, which is impossible in practice due to the real characteristics of a transistor. These imperfections are mainly represented by resistive and capacitive channel effects, which induce current and voltage overlapping and reduce the ideal 100% efficiency. This is illustrated in Fig. 13. Although the switching cannot be perfect, the SW class presents higher efficiency than the CW class at peak amplitude signals. Average efficiency is higher for AM signals if the AM information is recombined. The problem is to reintroduce the amplitude information of AM signals efficiently. One of the solutions in the case of SW PAs is that the transistor has an output voltage linearly dependant on the drain (for a MESFET) voltage due to the saturation, and this variation does not theoretically affect the high efficiency. This enables a supply modulation possibility in order to amplify non-constant modulated signals.
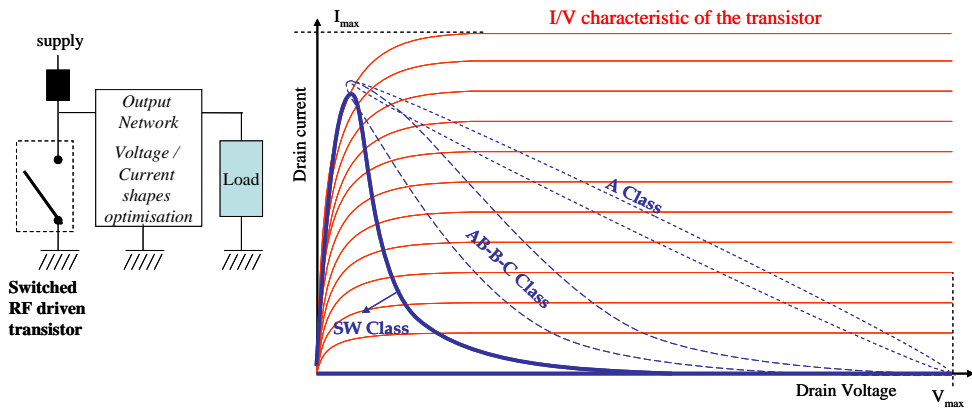
Fig. 13. Principle of SW classes (left) and Load line for CW and SW PA Classes (right).

Some SW classes can be considered for the emission of RF signals: class F and E. A class F PA is a saturated transistor, switched at the centre frequency, with additional resonating tanks in order to produce a sum of odd harmonics on the current and even harmonics on the voltage. This results in the generation of RF power only at the fundamental frequency, restoring the switching signal. It mathematically provides a null dissipated power (100% efficiency) but in practice the class F performance is limited by the non infinite number of resonating tanks. Another limitation of this PA class is the large number of shunt and series reactive elements necessary, all optimised for one frequency of operation. The tolerances of

the inductors and capacitors limit the performance of the PA due to its increase in sensitivity to the values of the reactive elements.

Class E PA design is different from class F. The number of shunt and series reactive elements (2 to 3) of the output network is limited and the calculus of optimum values is far more complex because it results from several hypotheses on the drain voltage and drain current shapes. These are: (i) perfect switching of the transistor at the centre frequency (duty cycle 50%) implying no overlapping of the drain voltage and drain current, (ii) perfect filtering of the fundamental frequency signal delivered to the load, (iii) null drain current in the transistor off state and null voltage in the transistor on state and (iv) null value of the drain voltage derivate when the transistor is switched on. Computations of these hypotheses discussed in (Sokal & Sokal, 1975); (Krauss et al., 1980); (Raab et al., 2003); (Diet et al., 2004-2008); (Robert et al., 2009) are summarized in Fig. 14, where $\theta = \omega t$.
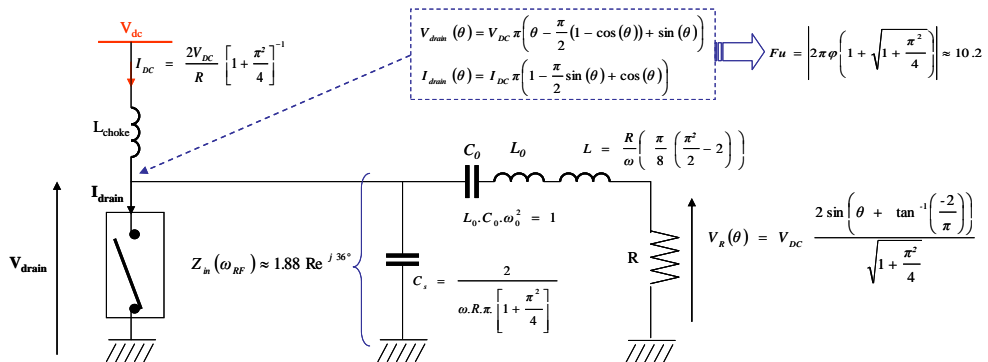

$$V_{drain}(\theta) = V_{DC}\,\pi\left(\theta - \frac{\pi}{2}(1 - \cos(\theta)) + \sin(\theta)\right)$$

$$I_{drain}(\theta) = I_{DC}\,\pi\left(1 - \frac{\pi}{2}\sin(\theta) + \cos(\theta)\right)$$

$$Fu = \left| 2\pi\varphi\left(1 + \sqrt{1 + \frac{\pi^2}{4}}\right)\right| \approx 10.2$$

$$I_{DC} = \frac{2V_{DC}}{R}\left[1 + \frac{\pi^2}{4}\right]^{-1}$$

$$L = \frac{R}{\omega}\left(\frac{\pi}{8}\left(\frac{\pi^2}{2} - 2\right)\right)$$

$$L_0 \cdot C_0 \cdot \omega_0^2 = 1$$

$$Z_{in}(\omega_{RF}) \approx 1.88\ \mathrm{Re}^{\,j\,36°}$$

$$C_s = \frac{2}{\omega.R.\pi\left[1 + \frac{\pi^2}{4}\right]}$$

$$V_R(\theta) = V_{DC}\ \frac{2\sin\left(\theta + \tan^{-1}\left(\frac{-2}{\pi}\right)\right)}{\sqrt{1 + \frac{\pi^2}{4}}}$$

Fig. 14. Class E basic design equations (Sokal &Sokal, 1975); (Kraus and al., 1980).

Theoretical equations determine particular shapes of the drain voltage and drain current for the class E operation. This is the typical reference for the PA designer. The large value of the factor *Fu*, particular to the class E, results in the PA being large, which is costly when integrating. Despite these design difficulties, a class E PA is very attractive because it provides very high efficiency regarding the number of reactive elements necessary for the output network. Some parasitic effects due to the transistor technology such as the drain capacitance (NL) and the drain resistance can be introduced in the determination of the (inductive) optimal impedance of the output network $Z_{in}(\omega)$. Works like those of (Diet et al., 2008) show that it is possible to determine some different output networks providing the same $Z_{in}(\omega)$. This was discussed for the first parallel inductance class E topology in (Grebennikov, 2002). Two class E topologies where compared in (Diet et al., 2008) for their potential use in high efficiency RF polar architecture, showing the keen interest in class E PAs for high data rate applications such as WiMAX.

To conclude the section on PAs for RF applications, one has to consider that the resulting efficiency in a given architecture is the criterion in the choice of a PA class. In the context of WiMAX transmitters, the linearization is mandatory whichever the class. High efficiency (SW) classes are favoured due to their high efficiency but the challenge shifts to the linearity of the amplified signal, expressed by the EVM, the ACPR and whether the emitted signal

spectrum respects the standard mask. Class E topology in polar architecture is currently the most popular solution.

4.4 Example of a Design for Mobile WiMAX

This sub-chapter presents and explains an example of a Mobile WiMAX transmitter. In the past years many transmitter architectures have been conceived (Masse, 2004); (Liu et al., 2005); (Pozsgay et al., 2008); (Yamazaki et al., 2008). All these transmitters are based on direct conversion architectures. Nowadays in Mobile WiMAX applications, these kinds of architectures are preferred, because of their high integration level. Most of the time they successfully fill specifications of the standard (noise, linearity and emitted power), but have reduced performance in terms of global efficiency. As explained in (Lloyd, 2006), WiMAX PAs are mainly in CW classes. They operate with 7 or 8 dB back-off to guaranty good linearity. The efficiency of such amplifiers used in Mobile WiMAX applications is about 18% (Eline et al., 2004). To address solutions to this issue, polar architecture associated with a class E amplifier seems to be a good trade-off between linearity and efficiency. The example presented here was extracted from (Robert et al., 2009). This transmitter is designed for WiMAX applications at 3.7 GHz. The first step is to conceive the Class E power amplifier, able to work at such a frequency. Figure 15 shows a serial inductor Class E topology (Sokal &Sokal, 1975). It is possible to calculate the optimum value of the Class E output network elements. In this case, the output of the transistor is supposed to be a short or an open circuit and the quality factor (Q) of C_0-L_0 is set to Q=5 for good switching.

$$C_0 = \frac{1}{(Q - 1.15249) \times R_1 \times \omega_0}$$

$$C_1 = \frac{0.1836}{R_1 \times \omega_0} - C_{DS}$$

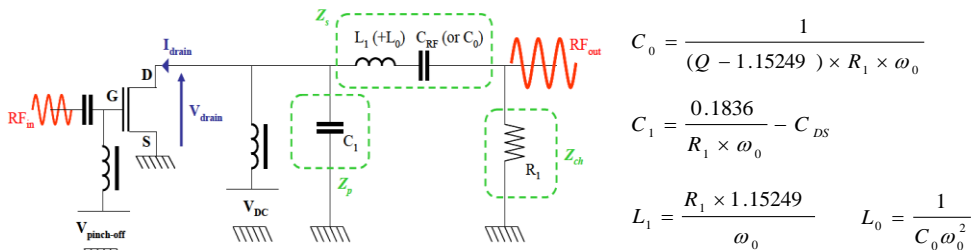$$L_1 = \frac{R_1 \times 1.15249}{\omega_0} \qquad L_0 = \frac{1}{C_0 \omega_0^2}$$

Fig. 15. Class E serial inductor topology and corresponding equations (Sokal & Sokal, 1975); (Robert et al., 2009).

The transistor used is a GaAs E-PHEMT, Avago ATF50189. The model introduces a drain to source capacitance C_{DS}. C_1 has to be calculated considering it would absorb the value of C_{DS}. An input matching network is designed keeping in mind that it should not filter the wide spectrum signal provided by the architecture (see Fig. 16), to preserve a constant envelope property. The amplifier offers drain efficiency (η) of 86.4% and 10.1 dB gain when the input is an 8 dBm 1-tone signal. As the amplifier will work at 3.7 GHz, a WiMAX signal is then injected at the polar architecture input (Suarez et al., 2008). Simulations parameters are fixed as: 10 MHz channel, 841 used subcarriers (1024 FFT size). The raw symbol rate is calculated using 64 QAM modulation to achieve the highest PAPR. Through the architecture, the signal provided to the amplifier is an 8 dBm constant envelope signal. First we observe the filtering behaviour of the amplifier (see Fig. 16). The overall gain is 3.5 dB whereas at the section with a 20 MHz bandwidth around the carrier the gain is 8.3 dB. The signal has been amplified

more at frequencies close to the carrier frequency than in the rest of the spectrum, due to the Class-E output network.
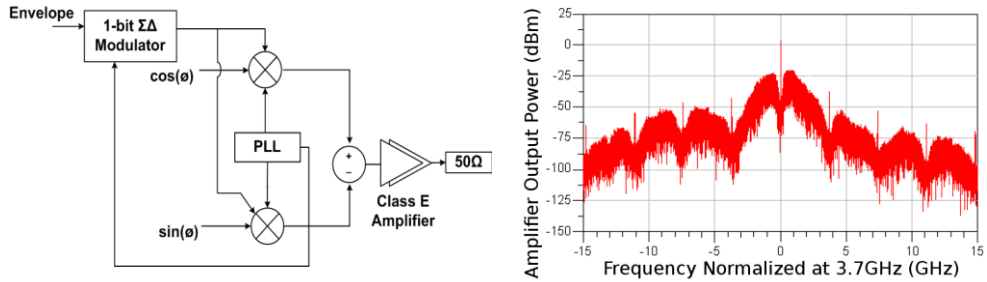

Fig. 16. ΣΔ Polar architecture with class E PA output spectrum.

The amplifier drain efficiency obtained using a high PAPR WiMAX (10 MHz) signal through a polar ΣΔ architecture at 3.7 GHz is 46.2% and the overall efficiency reaches 36.8%. This example stops at the frontier between amplifier and filter. It can be observed in Fig. 16 that filtering is still necessary after the amplifier. As the class E output network is dependant on the impedance presented to it (by filter and antenna), a co-design between theses three elements should be done to guaranty best performance (Diet et al., 2008).
This example shows that direct conversion architecture is not the only solution to Mobile WiMAX signal emission. A trade-off between integration, cost and performance, and thus efficiency and consumption needs to be made.

5. Filter Design Aspects and Solutions for Mobile WiMAX Radios

This sub-chapter is dedicated to the band pass filters required in WiMAX transmitters at the end of the transmission chain. The filter's requirements are related to the WiMAX RF architecture as was the case with the frequency synthesizer and the power amplifier. As presented in section 2.1, architectures based on decomposition and recombination of the signal offer high efficiency and become good candidates for WiMAX transmitters. In particular, polar architectures for wideband OFDM signals require a band-pass filter after the PA to filter the quantization noise introduced by envelope coders and to guarantee that the output respects the spectrum power mask (see Fig. 17).

5.1 WiMAX Filtering requirements

Mobile WiMAX channel profiles (Table 1) define frequency bands for mobile WiMAX and suggest the TDD mode, which is more suitable for mobile version of WiMAX. The RF filter in a TDD mode prevents the transmitter noise from self jamming the receiver since only one is on at any time (Eline et al., 2004). Furthermore, TDD mode implies that all the frequencies of the frequency range could be used for transmission at a given time. It is required to design one RF band-pass filter for the whole allocated frequency range within which any channel bandwidth could be selected (3.5, 5, 7, 8.75 or 10 MHz). According to Table 1 and depending on the chosen frequency range, RF filter bandwidths would be 15 MHz, 100 MHz, 190 MHz or 200 MHz.

The ratio between the filter bandwidth and its central frequency (*f*) serves to compare filter requirements and is also a useful criterion to choose the filter's technology. Table 2 summarizes the bandwidth and fractional bandwidth (*f*) for each frequency range.

Freq. Range GHz	2.3-2.4	2.305-2.32 / 2.345-2.36	2.496-2.69	3.3-3.4 / 3.4-3.8 / 3.4-3.6 / 3.6-3.8
Bandwidth- MHz	100	15 / 15	194	100 / - / 200 / 200
f - %	4.26	0.64	6.96	2.99 / - / 5.71 / 5.40

Table 2. Bandwidths and fractional bandwidth calculated from Mobile WiMAX profiles

The WiMAX standard establishes the maximum EVM accepted for WiMAX transmitters depending on modulation and coding. The most stringent EVM is -30 dB (3.16%) corresponding to a 64 QAM (3/4) modulation (IEEE, 2005). The EVM is calculated observing all the imperfections of the transmission chain blocks. Therefore, the maximum in-band ripple and group delay of the filter depend on this EVM value and on the imperfections generated by the other blocks of the architecture.

The filter's rejection is determined from the ACLR requirements which are set by national or regional regulatory bodies. This emission mask is often designed as a transmit spectrum mask. ACLR specifications may vary by region, band and channel bandwidth. For the particular case of Europe, the mask proposed by the European Telecommunications Standards Institute (ETSI) for the last WiMAX frequency range (> 3 GHz) is used as reference (ETSI, 2003). Fig. 17 presents the masks for a high complexity modulation format (as 64 QAM) which leads to the most stringent filtering constraints.

Because the filtering is carried out after the power amplification, the transmission filter must offer high power handling capability (high power dynamics and maximum power levels up to 23 dBm (Lloyd, 2006). The transmission filter for the WiMAX transmitter should also present low Insertion Losses (IL) to increase the whole architecture power efficiency. Moreover, as size and cost are critical parameters for manufacturers, it's desirable to use a filtering technology enabling integration.
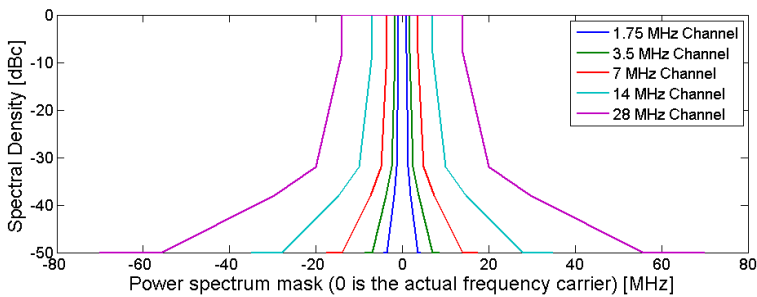

Fig. 17. Power Spectrum mask for a high complexity modulation format (ETSI, 2003).

5.2 Filtering Technologies

The most outstanding RF filtering technologies include LC Filters, Ceramic Filters, Surface Acoustic Wave (SAW) Filters, Bulk Acoustic Wave (BAW) Filters and Low Temperature Co-Fired Ceramic (LTCC) Filters. LC filters may support high frequencies and be integrated as a SoC; nevertheless, their main drawbacks are that they require too much area and have a

limited quality factor (Q). Ceramic filters offer low insertion losses (about 1.5 - 2.5 dB), high rejection (> 35 dB) and low cost. The downsides of ceramic filters are their significant size and integration limitations.

SAW filters are smaller than LC and Ceramic filters, but have limitations in frequency (up to 3 GHz). They support maximal power of 1 W which is acceptable for WiMAX mobile stations. Typical insertion losses vary between 2.5 and 3 dB and rejection can reach up to 30 dB. SAW filters cannot be IC integrated.

LTCC filters allow integrating high Q passive components; they offer low insertion losses, high maximal operation frequency and acceptable band rejection. LTCC filters are smaller than LC and Ceramic filters and can be integrated as System-on-Package.

BAW filters use Film Bulk Acoustic Resonators (FBAR) which present a high quality factor. They have low insertion loses (1.5 – 3 dB), significant rejection (≈ 40 dB) and high maximal operation frequency (up to 15 GHz). BAW filters can also deal with high output power (3 W). They are CMOS compatible and can be integrated "above IC", which means size reduction and package simplicity (Lakin, 2004). Besides, by employing wafer scale manufacturing using IC processing techniques BAW shows potential for low cost manufacturing.

5.3 Recent WiMAX Filters: BAW filters

BAW technology using Aluminium Nitride (AlN) piezoelectric material allows frequency operation up to 12 GHz. Each BAW filter is implemented with different sizes of FBARs which are associated on Ladder or Lattice topologies (Lakin, 2004). The particularity of this type of resonator is that each frequency response depends on the thin film piezoelectric thickness. Ladder filters are the most straight forward to implement because resonators may be individually optimized for reactance and central frequency during the design and manufacturing process. Ladder filters are single ended while lattice filters are double ended. Considering that in the transmitter architecture, the filter output is the antenna input, ladder topology is preferred to lattice topology because of its unbalanced signal and ease in tuning. Filters are preceded by HPA unbalanced output as well. The Butterworth Van Dyke (BVD) model is an electric circuit model to characterise FBAR resonators. The BVD equivalent circuit of the crystal resonator is shown in Fig. 18.

$$C_p = \frac{\varepsilon_0 \varepsilon_r A}{d}; \quad C_s = \frac{8 k_t^2 C_p}{\pi^2}$$

$$L_s = \frac{\pi^3 V_a}{8 w_s^3 \varepsilon_0 \varepsilon_r A k_t^2}; \quad R_s = \frac{L_s w_s}{Q}$$

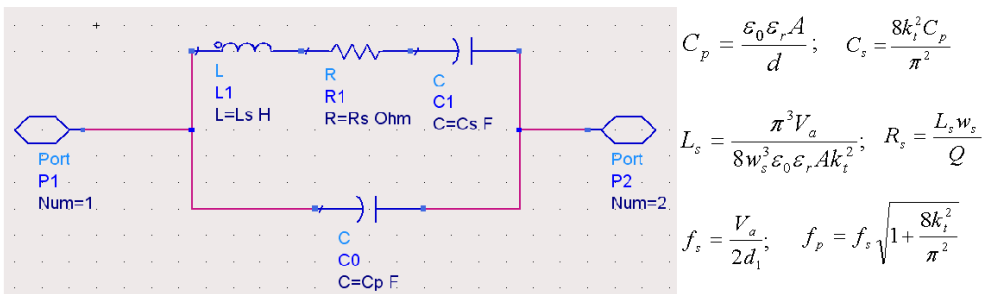$$f_s = \frac{V_a}{2 d_1}; \quad f_p = f_s \sqrt{1 + \frac{8 k_t^2}{\pi^2}}$$

Fig. 18. FBAR resonator – BVD model.

The resonator is in the form of a simple capacitor which has a piezoelectric material for the dielectric layer and suitable top and bottom metal electrodes. The simplified equivalent

circuit of the piezoelectric resonator has two arms. C_p is the geometric capacitance of the structure and the R_s, L_s, C_s portion of the circuit is called the "motional arm," which arises from the mechanical vibrations of the crystal. The series elements R_s, L_s, C_s which are controlled by the acoustic properties of the device, account for the motional loss, the inertia and the elasticity respectively. These parameters can be calculated from equations presented in Fig. 18. ε_r is the material's relative permittivity (10.59 for the AlN), k_t^2 is the electromechanical coupling constant (6% for the AlN), V_a is the acoustic material velocity (10937 for the AlN), A is the surface area of the electrodes, d is the thickness of the piezoelectric material, and Q is the quality factor. w_s and w_p correspond to 2π times the resonance (f_s) and anti-resonance (f_p) frequencies of the resonator.

Thickness of series and shunt resonators can be different; d_1 refers to the series and d_2 to the shunt resonator thickness. It can be observed that only two parameters can be optimized in order to design a band-pass filter, these are surface area A (expressed as $l \times l$) and resonator thickness (d_1 and d_2). A series and shunt resonator constitute a stage. In order to achieve desired responses and higher out-of-band rejection, stages can be cascaded; each additional stage (a couple of series-shunt resonator) increases the filter order by one, therefore a 6 resonator ladder filter is a third order filter.

An example of a WiMAX filter in the 3.6 – 3.8 GHz frequency band was proposed in (Suarez et al., 2008). The emission filter in this case has a bandwidth of 200 MHz. From Fig. 17 it can be observed that the out-of-band rejection must be 50 dB at twice the channel bandwidth (20 MHz from the edge for a 10 MHz channel).

Resonator fabrication constraints require that the thickness is between 1 µm and 6.5 µm and surface areas between 10 µm * 10 µm and 600 µm * 600 µm. Thickness of the series and shunt resonators are 2.79 µm and 2.88 µm respectively. The transmission response of the WiMAX designed filter, resonators lengths and filter's insertion losses and rejection are presented in Fig. 19.
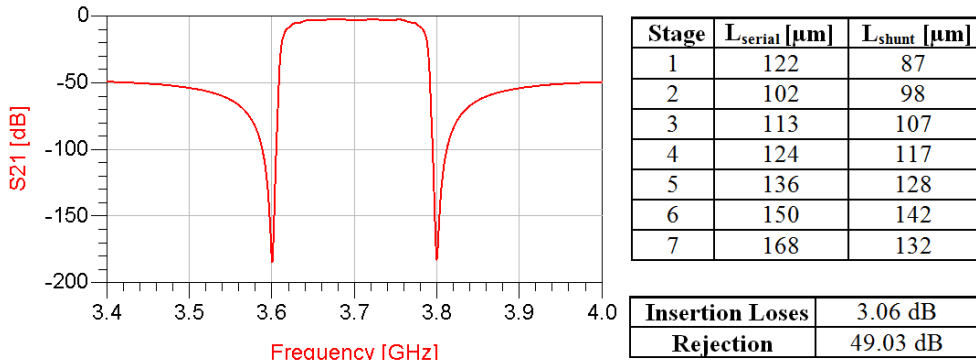

Stage	L_{serial} [µm]	L_{shunt} [µm]
1	122	87
2	102	98
3	113	107
4	124	117
5	136	128
6	150	142
7	168	132

Insertion Loses	3.06 dB
Rejection	49.03 dB

Fig. 19. [S_{21}] parameter of a WiMAX RF filter using BAW technology (7th order ladder).

5.3 Recent WiMAX Filters: Other examples.

Some other examples of band pass filters for WiMAX using LTCC technologies have been published recently. For example (Kim et al., 2008) proposes a Quad band module for Wi-Fi/WiMAX applications where, for the WiMAX mode, the insertion loss is less than 4.6 dB at 3.5 GHz and the attenuation is more than 26 dB. In the same frequency band an LTCC

filter has also been proposed by (Accute), it has about 200 MHz of bandwidth, 2.7 dB IL, less than 1 dB of ripple and more than 30 dB of attenuation.

A whole WiMAX System-in-Package based on LTCC has also been proposed by (Heyen et al., 2008). This is a single band approach in the frequency band of 2.5-2.7 GHz and comprises the complete passive and active RF front-end plus the transceiver RFIC for up- and down-conversion to base band. The RF transmission filter provides harmonics and spurious rejections better than 40 dB.

6. Other Design Aspects

In previous sections the performance of the baseband and radiofrequency parts of a WiMAX transmitter were discussed. These are the parts of the transmitter between the digital electronics and the antenna. The importance of the choice of architecture has been demonstrated, as have the impacts of key elements such as frequency synthesizers, power amplifiers and emission filters. This section points out the considerations to add for a global design of such a transceiver regarding the performance of Digital to Analogue Converters (DACs) and antennas at these frequencies.

6.1 Digital and analogue

The DAC enables baseband signal generation after the shaping filter. It should have low distortion, sufficient bandwidth and low consumption. DACs are used in conventional architecture for I and Q paths generation and in polar architecture for phase (I and Q) and envelope paths. In polar architecture there is one DAC more and the required bandwidth is extended due to the non-linear processing when generating the "phase" and the "magnitude/envelope" of the signal. Also, the coding of the envelope is an additional restriction in terms of speed for the $\Sigma\Delta$. As the Signal to Noise Ratio (SNR) of the signal is admitted to grow with the number of bits and bandwidth, these specifications are mandatory limiting factors. Nowadays, some converters work in the range of several bits near a GHz and around 12 to 20 bits near a MHz.

Due to the conclusions of previous sections, the example presented here is the simulation of a polar architecture for an OFDM signal with 64 sub-carriers (typically IEEE802.11a). The symbol rate is 20 MHz and the carrier frequency is 5.2 GHz but can be shifted to 3.7 GHz without altering the observations because the DAC influences are introduced on the baseband processing. Figure 20 presents the emitted spectrum in an ideal polar/EER transmitter simulation with limitation of the bandwidth on the envelope and phase signals. Limits are three times the symbol rate for the envelope and seven times for the phase ones. The mask of the IEEE 802.11a standard is added on the same figure and it is noticeable that the emitted spectrum is not far from the limit. The most limiting parameters are the phase signals.
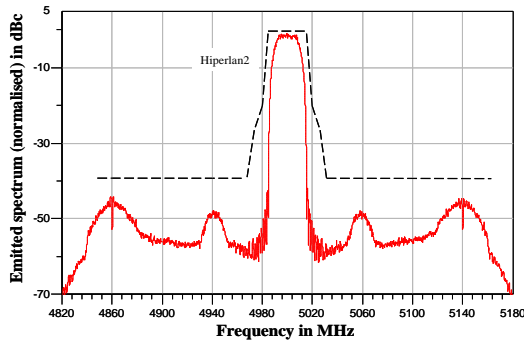
Fig. 20. Emitted spectrum of a 20 MHz OFDM Hiperlan 2 signal with band width limitations of 60 MHz (envelope signal) and 140 MHz (I and Q phase signals). The EVM rms is 0.2%.

This implies a high bandwidth for the baseband signals generation. The resolution will therefore be strongly impacted because the higher the bandwidth, the lower the resolution (without consideration of power consumption). The second step of our example is to limit the number of bits for the signal representation. Here the envelope is coded in either signed or unsigned format (depending on the specification/complexity of the hardware part of the system) and without a clipping that could have reduced the needed dynamic for the envelope but at the cost of an EVM increase. Results in the classical architecture case and polar one are presented on Fig. 21.

EVM / EVM max (% rms)	7 bits	6 bits	5 bits	4 bits	6 bits (envelope unsigned)	8 bits (2'complement)
I and Q paths for OFDM sig.	0.3 / 0.5	0.6 / 0.9	1.2 / 1.8	2.8 / 5		
I and Q paths OFDM phase sig.	0.1 / 0.2	0.4 / 0.7	0.7 / 1.3	1.6 / 2.5	0.9 / 1.8	0.4 / 1.1
Envelope default is unsigned format	0.2 / 0.3	0.4 / 0.5	0.6 / 0.9	1.3 / 2.1		

Fig. 21. Results of resolution limitation for an OFDM Hiperlan 2 transmitter.

The limitation of the resolution with an acceptable EVM of 0.5% rms (without any other architecture imperfection) is at the edge of the actual DACs performance, which is 8 bits with a supposed bandwidth of tens of MHz. To realistically illustrate the influence of both parameters introduced in the simulation, we show in Fig. 22 the simulation of the polar/EER architecture with DACs of 8 bits resolution and with the same bandwidth limitations as shown in Fig. 20. The emitted spectrum is compared with the same mask and the constellation and EVM are presented. The results show an acceptable EVM below 0.5% rms and the spectrum is, in conclusion, the main criterion for characterizing the DAC impact in the architecture.
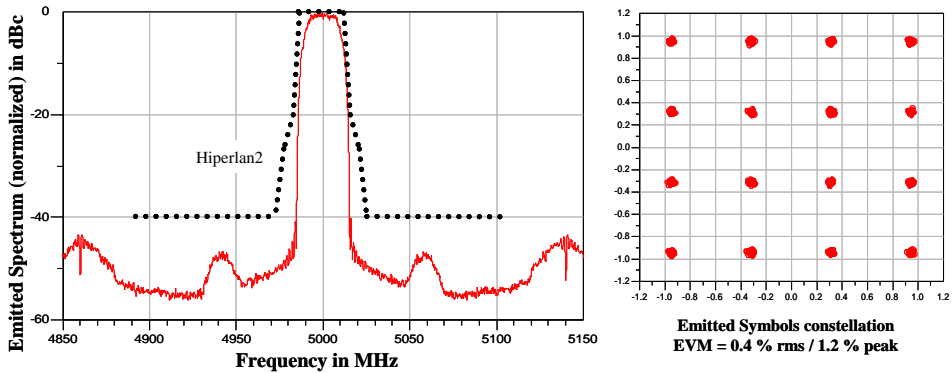
Fig. 22. Emitted spectrum and constellation for an OFDM Hiperlan 2 transmitter with bandwidth limitations of 60 MHz (envelope signal) and 140 MHz (I and Q phase signals), and an 8 bit DAC.

6.2 Antennas

Antennas for handsets have to be adapted to the difficult environment of indoor mobility (omni-directivity or wide radiation lobe, polarization) while maintaining a small size and cost. Solutions are, for example, helicoidal antennas, patch or planar antennas with tuned slot; often with a ground reflector in the case of mobile phone application to avoid radiations toward the user and coupling to the circuit (in this case the ground plane is a kind of "shield"). The use of antenna diversity or Multiple Input Multiple Output (MIMO) benefits the receiver and significantly increases its performance, but this is a challenge in terms of power consumption for a battery operated system (additional RF sub-systems). In the case of the integration of multiple wireless systems, it is important to focus on antenna integration and especially multi-band or wideband antennas. Whatever the standards considered, diversity of antennas and antennas for multiple standards are research topics for systems offering mobile communications and connectivity (such as WiMAX). In conclusion, integrated low cost antennas are to be investigated for this type of system with regards to the standards specifications (bandwidths, propagation environment) and with architectural considerations (size, cost, consumption in the case of MIMO).

7. Conclusion

As a result of flexible and multi-band radio operation, the Mobile WiMAX standard presents a challenge for every stage of the RF front-end. New techniques and mechanisms for linear and high efficient transmission have been discussed, along with their advantages and limitations. The ultimate goals are high degree of RF integration into cheap CMOS technology and high power efficiency along with linearity. At this point, the polar based architecture can offer high performance solutions for high PAPR wideband signals, while providing high efficiency due to switched mode amplification.

It has been shown that the RF filtering, which is required after the power amplifier presents a significant challenge for RF designers. Appropriate filtering technologies have been presented, including current examples of WiMAX filters.

Moreover, signal deterioration resulting from the frequency synthesizer's phase noise contribution has been discussed as well, along with solutions for low noise high speed synthesis.

8. References

Accute Microwave. Specification of LTCC Filter - LF43B3500P34-N42.

Armada, G. A. (2001). Understanding the effects of phase noise in orthogonal frequency division multiplexing. *IEEE Trans. Broadcast.*, Vol. 47, No. 2, pp. 153-159, June 2001.

Baudoin, G.; Bercher, JF.; Berland, C.; Brossier, JM.; Courivaud, D.; Gresset, N.; Jardin, P.; Bazin-Lissorgues, G.; Ripoll, C.; Venard, O.; Villegas. M. (2007). *Radiocommunications Numériques : Principes, Modélisation et Simulation*. Dunod, EEA/Electronique, 672 pages, 2ème édition 2007.

Choi, J.; Yim, J.; Yang, J.; Kim, J.; Cha, J.; Kang, D.; Kim, D. ; Kim, B. (2007). A ΣΔ digitized polar RF transmitter. *IEEE Trans. on Microwave Theory and Techniques,* Vol. 52, No. 12, 2007, pp 2679-2690.

Cimini, L. J. (1985). Analysis and simulation of a digital mobile channel using orthogonal frequency division multiplexing. *IEEE Trans. Commun.*, Vol. 33, No. 7 (July 1985), pp. 665–675.

Cox, D. C. (1974). Linear amplification with non-linear components, LINC method. *IEEE transactions on Communications,* Vol. COM-23, pp 1942-1945, December 1974.

Crowley et al. (1979). Phase locked loop with variable gain and bandwidth. *U.S. Patent 4,156,855,* May 29, 1979.

Diet, A.; Berland, C.; Villegas, M.; Baudoin, G. (2004). EER architecture specifications for OFDM transmitter using a class E power amplifier. *IEEE Microwave and Wireless Components Letters (MTT-S),* Vol.-14 I-8, August 2004, pp 389-391, ISSN 1531-1309.

Diet, A.; Robert, F.; Suárez, M.; Valenta, V.; Andia Montes, L.; Ripoll, C.; Villegas, M.; Baudoin. (2008) G. Flexibility of class E HPA for cognitive radio, *Proceedings of IEEE 19th symposium on Personal Indoor and Mobile Radio Communications, PIMRC 2008,* 15-18 September, Cannes, France. CD-ROM ISBN 978-1-4244-2644-7.

Diet, A.; Villegas, M.; Baudoin, G. (2008). EER-LINC RF transmitter architecture for high PAPR signals using switched Power Amplifiers. *Physical Communication, ELSEVIER*, ISSN: 1874-4907, V-1 I-4, December 2008, pp. 248-254.

Eline, R.; Franca-Neto, L.M.; Bisla, B. (2004). RF System and circuit challenges for WiMAX. *Intel Technology Journal,* Vol. 08, Issue 03 2004

ETSI. (2003). European Standard, Telecommunications Series, *ETSI 301021 V1.6.1*, 2003.

Grebennikov, A. (2002). Class E high efficiency PAs : Historical aspect and future prospect. *Applied Microwave and Wireless*, July 2002, pp 64-71.

Herzel, F.; Piz, M. and Grass, E. (2005). Frequency synthesis for 60 GHz OFDM systems, *Proceedings of the 10th International OFDM Workshop (InOWo'05),* Hamburg, Germany, pp. 303–307, 2005.

Heyen, J.; Yatsenko, A.; Nalezinski, M.; Sevskiy, G.; Heide, P. (2008). WiMAX System-in-package solutions based on LTCC Technology, *Proceedings of COMCAS 2008*.

IEEE Standard 802.16e. (2005). Air interface for fixed and mobile broadband wireless access systems amendment 2: physical and medium access control layers for combined fixed and mobile operation in licensed bands, 2005.

Kahn, L. R. (1952). Single sideband transmission by envelope elimination and restoration, *Proceedings of the I.R.E., 1952, pp. 803-806*.

Keliu, S. and Sanchez-Sinencio, E. (2005). *CMOS PLL Synthesizers: Analysis and Design*, Springer, 0-387-23668-6, Boston.

Kim, D.; Dong Ho Kim; Jong In Ryu; Jun Chul Kim; Chong Dae Park; Chul Soo Kim; In Sang Song. (2008). A quad-band front-end module for Wi-Fi and WiMAX applications using FBAR and LTCC Technologies, *Proceedings of APMC 2008.*

Krauss, H. C.; Bostian, C. W. and Raab, F. H. (1980). *Solid State Radio Engineering*, Wiley, 047103018X, New York.

Kyoungho W.; Yong L.; Eunsoo N.; Donhee, H. (2008). Fast-lock hybrid PLL combining fractional-N and integer-N modes of differing bandwidths. *IEEE Journal of solid state circuits*, Vol. 43, No. 2, pp. 379-389, Feb. 2008

Lakin, K. (2004). Thin film BAW filters for wide bandwidth and high performance applications, *IEEE MTT-S* 2004.

LIM, D.-W, et al. (2005). A new SLM OFDM Scheme With Low Complexity for PAPR Reduction. *IEEE Signal Processing Letters*, Vol. 12, No. 2, February 2005, pp. 93-96.

Liu, H.; Chin, H.; Chen, T.; Wang, S.S. Lu. (2005). A CMOS transmitter front-end with digital power control for WiMAX 802.16e applications, *Microwave Conference Proceedings, APMC 2005. Asia-Pacific Conference Proceedings,* Vol. 3.

Lloyd, S. (2006). Challenges of mobile WiMAX RF transceivers. *Solid-State and Integrated Circuit Technology, 2006. ICSICT '06.* 23-26 Oct. 2006.

Masse, C. (2006). A 2.4 GHz direct conversion transmitter for WiMAX applications, *Radio Frequency Integrated Circuits Symposium,* 11-13 June 2006.

Mäuller, H. S. & Huber, J.B. (1997). A novel peak power reduction scheme for OFDM, *Proc. of the Int. Symposium on Personal, Indoor and Mobile Radio Communications PIMRC'97*, Sept. 1997, Helsinki, Findland, pp. 1090-1094.

Memmler, B.; Gotz, E.; Schonleber, G. (2000). New fast-lock PLL for mobile GSM GPRS applications, *Solid-State Circuits Conference*, ESSCIRC 2000.

Muschallik, C. (1995). Influence of RF oscillators on an OFDM signal. *IEEE Trans. Consumer Electronics*, Vol. 41, No. 7, pp. 592–603, Aug 1995.

Nee, R. & Prasad, R. (2000). *OFDM for wireless multimedia communications*, Artech House, 2000.

Nielsen, M.; Larsen, T. (2007). Transmitter architecture based on ΔΣ modulation and switch-mode power amplification. *IEEE Trans. on Circuits and Systems II*, 2007, Vol. 54, No. 8, pp. 735-739.

Pozsgay, A.; Zounes, T.; Hossain, R.; Boulemnakher, M.; Knopik, V.; Grange, S.; A fully digital 65nm CMOS transmitter for the 2.4-to-2.7 GHz WiFi/WiMAX bands using 5.4 GHz ΔΣ RF DACs, *Proceedings of ISSCC 2008,* pp: 360-619.

Raab, F. et al. (2003). RF and microwave PA and transmitter technologies. *High Frequency Electronics,* May-November 2003, pp 22-49.

Robert, F.; Suarez, M.; Baudoin, G.; Villegas, M.; Diet, A. (2009). Analyse de l'influence du codage d'enveloppe sur les performances de l'amplificateur classe E d'une architecture polaire, *XVI Journées Nationales Micro-ondes, JNM*, mai 2009, Grenoble, France.

Robert, F.; Suarez, M.; Diet, A.; Villegas, M.; Baudoin, G. (2009). Study of a polar sigma-delta transmitter associated to a high efficiency switched mode power amplifier for mobile WiMAX, *Proceedings of IEEE WAMICON* 2009, 20-21 Apr.2009

Sokal, N. and Sokal, A. (1975). Class E, a new class of high efficiency tuned single ended switching PAs. *IEEE journal of Solid State Circuits, Vol. 10, No. 3, Juin 1975, pp 168-176.*

Suarez, M.; Villegas, M.; Baudoin, G. (2008). Front end filtering requirements on a mobile cognitive multi-radio transmitter, *Proceedings of the 11th International Symposium on wireless Personal Multimedia Communications,* 8-11 Sept. 2008, Saariselka, Finlande.

Suarez, M.; Valenta, V.; Baudoin, G.; Villegas, M. (2008). Study of a modified polar sigma-delta transmitter architecture for multi-radio applications, *Proceedings of EuMW, European Microwave Week,* 27-31 Oct. 2008, Amsterdam, Netherlands.

Tellado, J. (2000). *Multicarrier Modulation with Low PAR*, Kluwer Academic Publishers, 2000

Valenta, V.; Villegas, M.; Baudoin, G. (2008). Analysis of a PLL based frequency synthesizer using switched loop bandwidth for mobile WiMAX, *Proceedings of the 18th International Conference Radioelektronika 2008*, pp. 127-130. ISBN: 978-1-4244-2087-2.

Valenta, V.; Marsalek R.; Villegas, M.; Baudoin, G. (2009). Dual mode hybrid PLL based frequency synthesizer for cognitive multi-radio applications, *submitted for WPMC'09.*

Villegas, M.; Berland, C. ; Courivaud, D. ; Bazin-Lissorgues, G. ; Picon, O. ; Ripoll, C. ; Baudoin, G. (2007). *Radiocommunications Numériques : Conception de circuits intégrés RF et micro-ondes*. Dunod, EEA/Electronique, 464 pages, 2ème édition 2007.

Yamazaki, D.; Kobayashi, N.; Oishi, K.; Kudo, M.; Arai, T.; Hasegawa, N.; Kobayashi, K. (2008). 2.5-GHz fully-integrated WiMAX transceiver IC for a compact, low-power consumption RF module, *Radio Frequency Integrated Circuits Symposium, RFIC 2008,* June 17 2008-April 17 2008.

Qiyue Zou, Tarighat, A. and Sayed, A.H. (2007). Compensation of phase noise in OFDM wireless systems. *IEEE Trans. Signal Processing*, Vol. 55, No. 11, pp. 5407-5424, Nov 2007.

WiMAX Forum™ Mobile System Profile 3 Release 1.0 Approved Specification 4 (Revision 1.7.1: 2008-11-07).